Journal of Naval Architecture and Marine Engineering
June, 2017
http://dx.doi.org/10.3329/jname.v14i1.27967 *http://www.banglajol.info*

A PRELIMINARY STUDY OF FLUID-DYNAMIC LOADS ON A PLANE SURFACE BENEATH A CIRCULAR CYLINDER IN THE SUBCRITICAL FLOW REGIME

Jian-Cheng Cai [1*], Jie Pan [2], Shi-Ju E[1], Wei-Dong Jiao[1] and Dong-Yun Wang[1]
[1]Department of Mechanical Engineering, College of Engineering, Zhejiang Normal University, Jinhua 321004, China, *Email: cai_jiancheng@foxmail.com
[2]School of Mechanical and Chemical Engineering, The University of Western Australia, Crawley WA 6009, Australia, jie.pan@uwa.edu.au

Abstract:

This paper studies the fluctuating forces on a plane surface beneath a circular cylinder in the subcritical flow regime using two-dimensional computational fluid dynamics (CFD) approach. The turbulent flow fields were calculated via numerical solutions of the Navier–Stokes (N–S) equations without a turbulence model (laminar flow computation), large eddy simulation (LES), and Reynolds-Averaged N-S equations (RANS) approach with the shear-stress transport (SST) turbulence model. The primary goal is to evaluate the correctness, accuracy, and applicability of 2-D approximation of turbulence simulation with different approaches for subcritical flow regime (Re=5000). Some preliminary knowledge of the forces on the plane which is important in studying scours and flow-induced vibration in ocean engineering is obtained. Results show that the laminar approach with high mesh resolution can adequately simulate turbulent flows at this moderate Reynolds number. Specially, the fluctuating forces on the plane surface due to the flow are significant within three times the cylinder diameter in the downstream, and within one cylinder diameter in the upstream of the cylinder. The pressure fluctuations are approximately two orders of magnitude larger than the shear stress fluctuations. In the frequency domain, the fluctuating forces are significant under twice the vortex-shedding frequency. Within one cylinder diameter in the downstream and upstream regions of the cylinder, the pressure fluctuations on the plane surface are well correlated whereas the shear stress is not so well correlated.

***Keywords*:** Fluctuating forces, surface pressure, surface shear stress, unsteady flow, circular cylinder, wall proximity, vortex shedding, numerical simulation

NOMENCLATURE

D	diameter of the cylinder
$k=\overline{u_i'u_i'}/2$	turbulent kinetic energy per unit mass
p	pressure
t	time
u_0	free-stream flow velocity
u_i	velocity components
x_i	space coordinate components

Greek symbols

δ_{ij}	Kronecker delta
ε	turbulent kinetic energy dissipation rate
μ	dynamic viscosity
μ_t	turbulent or eddy viscosity
ν	kinematic viscosity
ρ	fluid density

1. Introduction

Flow around a circular cylinder has been a subject of much research. Particularly important aspects are the periodic fluctuating cross-flow (lift) and in-line (drag) forces that result from the vortex shedding of the flow, which are the sources of flow-induced oscillations of a cylindrical structure. Although as a classic topic in fluid mechanics, it is actually quite a complex problem. As the Reynolds number Re=Du_0/ν increases, the flow pattern around the cylinder changes (Sumer and Fredsoe, 2006). When Re < 5, no flow separation occurs, and for 5 < Re < 40, a fixed pair of vortices forms in the wake of the cylinder. When the Reynolds number is further increased, the wake becomes unstable and vortex shedding occurs. The flow of the wake behind the cylinder

1813-8535 (Print), 2070-8998 (Online) Received on: June, 2016

enters the turbulence regime when Re > 300; however, the boundary layer around the cylinder surface is laminar. With a further increase in Re up to 3×10^5, the transition to turbulence occurs in the boundary layer itself. For $300 < Re < 3\times10^5$, the flow regime is known as the subcritical flow regime with the laminar boundary layer separation, where $Re = 3\times10^5$ marks critical flow, and $Re > 3.5\times10^5$ defines the supercritical flow regime with the turbulent boundary layer separation.

A plane boundary beneath the cylinder will add further complexity to the flow structure around the cylinder, as the plane boundary influences the flow via the kinematic and kinetic constraints on its rigid surface and the growing boundary layer along the surface. It is well known that the Re, the gap-to-diameter ratio (G/D) and the ratio of the incident boundary layer thickness to the diameter (δ/D) are crucial to the flow pattern around the cylinder. Here, G is the minimum distance between the bottom of the cylinder and the plane wall, and δ is the thickness of boundary layer of the inlet flow upstream of the cylinder.

It is generally accepted that the vortex motion behind the cylinder and close to the boundary wall is suppressed for $G/D < 0.3$, and that the flow interference between the cylinder and the plane boundary becomes very weak when $G/D > 1.0$ (Sumer and Fredsoe, 2006). These observations were also confirmed in flow field visualizations by Oner *et al.* (2008). Oner *et al.* (2008) also measured the distribution of mean pressure around the cylinder and along a plane boundary, and their results showed that along the plane boundary the pressure is positive at the upstream part of the cylinder and negative downstream, and that the mean pressure over the cylinder showed that the cylinder experienced a net positive lift force, i.e., the force pushes the cylinder away from the plane wall. Price *et al.* (2002) showed that the onset of vortex shedding can only be observed for $G/D > 0.5$, while it is completely suppressed when $G/D < 0.125$, in the Reynolds number range of 1200 to 4960. In the intermediate region, $0.125 < G/D < 0.5$, the flow is similar to that for $G/D < 0.125$, but there is a pronounced pairing between the lower shear layer shed from the bottom side of the cylinder and the wall boundary layer.

Kazeminezhad *et al.* (2010) numerically investigated the effects of the boundary layer of the plane boundary on the vortex shedding frequency of the flow around the cylinder and the forces acting upon the cylinder when exposed to a steady current (at Re = 7000 and 9500) by solving the 2-D Reynolds-averaged Navier–Stokes (RANS) equations with the k–ε turbulence model. Their model slightly over-predicted the mean force coefficients and Strouhal number. It was concluded that the mean force coefficients and the root-mean-square (RMS) lift coefficient are strongly affected by the gap-to-diameter ratio while the Strouhal number is slightly affected by the gap ratio.

Ong *et al.* (2010) performed a numerical simulation of flow around a circular cylinder close to a flat seabed at high Reynolds numbers ($Re = 1.31\times10^4$ and 3.6×10^6) using a 2-D standard k–ε model. They found that overall the employed approach is suitable for design purposes at high Reynolds numbers, but that there existed differences between the experimental and numerical results.

Tutar and Holdø (2001) performed 2-D simulation of flow around a cylinder in the subcritical regime using a k–ε turbulence model and a large eddy simulation (LES). They found that LES methods with the sub-grid scale (SGS) model yielded much more realistic pictures of the flow's vortex shedding in the transitional flow regime, but slightly overestimated critical flow parameters.

Liang *et al.* (2005) studied the performance of the standard k–ε, Wilcox k-ω, and Smagorinsky's SGS turbulence models against the flow around a circular cylinder located 0.37 diameters above a rigid surface. They demonstrated that an LES with Smagorinsky's SGS model predicted much stronger vortex shedding as well as the fluctuation velocities and the RMS lift coefficient.

Previous work on flow around a cylinder near a plane surface had largely focused on the forces on the cylinder. However, there appears to be a need to understand the fluctuating forces on the plane surface caused by the unstable flow generated by the flow–cylinder interaction, as fluctuating pressure and shear stress on a surface are important sources of surface vibration and sound radiation in structural acoustics (Liu *et al.*, 2012).

This paper focuses studying the fluctuating forces on the surface of a rigid plane below a cylinder. The study is undertaken via a 2-D simulation of unsteady flow fields around a cylinder above a plane surface at two different gap-to-diameter ratios ($G/D = 0.3$ and 1.0) using different turbulence approaches. It is generally accepted that $G/D = 0.3$ corresponds to the critical situation where vortex shedding begins, while $G/D = 1.0$ is a case where the influence of the plane surface on the flow field behind the cylinder can be ignored (Price *et al.*, 2002). This study is limited to subcritical Reynolds number, Re = 5000, because the corresponding flow patterns are relatively simple for explaining the features of the surface forces.

A numeric solution of the Navier–Stokes (N–S) equations without any turbulence model (*i.e.*, the laminar approach in commercial CFD packages), the RANS equations with the *k–ω* shear-stress transport (SST) model, and an LES approach with Smagorinsky's SGS model were used for this study. The numerical results were compared to existing experimental results. It should be pointed out that the turbulent flow around the cylinder is intrinsically three dimensional, nevertheless the 2-D simulation in flow around cylinders still has its applications because of its low calculation effort, especially of the RANS approach (Rahman *et al.*, 2007, Stringer *et al.*, 2014), where the *k-ε* Realizable and *k-ω* SST turbulence models were used.

The application of 2-D LES seems to be a controversial issue. Some researchers argue that the 2-D LES is inaccurate (Murakami and Mochida, 1995, Rodi, 1993), while some studies show quite good results by using a fine grid resolution (Bouris and Bergeles, 1999, Tutar and Holdø, 2001).This contradiction can be explained by different conditions, under which the mentioned results have been obtained. It gives us the possibility to suppose that in the case of subcritical flow mode especially of low Reynolds number flows, when boundary layers developing over cylindrical surface are laminar and turbulence in the wake behind cylinder just begins to develop, its spanwise direction (along the cylinder axis) component is not so effective or slightly correlated with other dominant directions of flow spreading, thus the 2-D level of turbulence approximation for this special case can be acceptable. This suggestion motivates the primary goal of this research: to evaluate the correctness, accuracy, applicability and performance of such 2-D level of approximation of turbulence simulation with different approaches for subcritical flow mode, and to obtain some preliminary knowledge of the forces on the plane which is important in studying scours and flow-induced vibration in ocean engineering.

2. Mathematical Formulation

2.1 Problem Description

A schematic sketch of the flow around a circular cylinder close to a plane surface is shown in Fig. 1. The diameter of the cylinder is D = 0.01 m. The upper boundary of the mesh is located at a distance from 8.7D from the top of the cylinder. This ensures that the boundary of the mesh has a negligible effect on the flow around the cylinder and the plane surface. The gap between the bottom of the cylinder and the plane surface is denoted by G, which is 0.3D or 1.0D related to G/D = 0.3 or 1.0. The flow inlet is located 13D upstream from the center of the cylinder, and the flow outlet is located at 32D. These distances are sufficient to eliminate far-field effects of the flow upstream and downstream of the cylinder. The computational region in the downstream dimension is larger than the regime enclosed by the inlet and symmetric boundaries, as suggested by Ong *et al.* (2010), in order to further reduce the influence of the outlet, because backflow usually occurs in the near downstream region owing to the vortex motion carried out by the main flow.

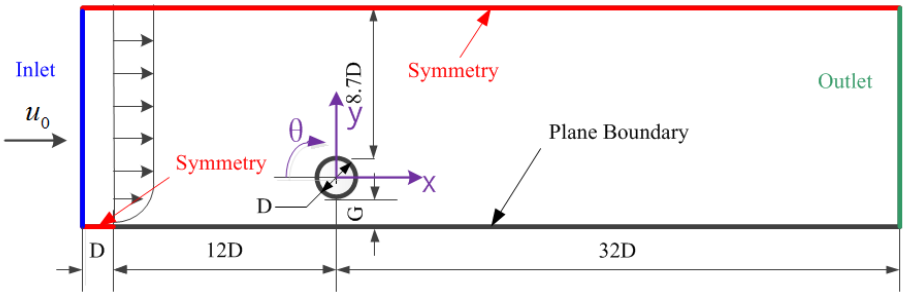

Fig. 1: Schematic of the flow region.

Unlike most previous studies in which the inlet velocity distribution, including the boundary layer shape, was given, this study applies a uniform velocity distribution at the inlet with a magnitude of u_0 = 0.5 m/s. The dynamic viscosity $\mu = 10^{-3}$ Pa·s, and the density ρ = 1000 kg·m^{-3}, thus the kinematic viscosity $\nu = 10^{-6}$ m^2/s and Re=Du_0/ν=5000. After a distance of 1D along the flow direction, the incoming flow hits the plane surface and a boundary layer is thereafter generated along the leading point of the plane. The ratio of boundary layer thickness to the cylinder diameter at a distance of 5D in front of the cylinder center, obtained from the computational fluid dynamics (CFD) simulation, is $\delta/D \approx 0.2$. One can expect that the interactions between the boundary layer and flow around the cylinder will be appreciable for G/D = 0.3, and very weak for G/D = 1.0.

Three mesh schemes with quadrilateral cells of different sizes were constructed. The total cell numbers of these three mesh schemes are approximately 80,000, 300,000, and 1,100,000, and some representative mesh pictures of G/D = 0.3 are shown in Fig. 2. Much finer meshes are used in the near-wall regions in order to keep the non-

dimensional wall distance y-plus of ~1 at most near-wall vertexes. The y-plus is obtained from the Reynolds number, using the wall distance and the friction velocity as the characteristic length and velocity. Lee *et al.* (2014) carried out a 3-D LES calculation of the flow past a cylinder at Re = 5000 with the span length of 2*D* using six different mesh levels). Judging from the y-plus values, it can be predicted that the fine mesh scheme in the paper is equivalent to the finest mesh level therein.

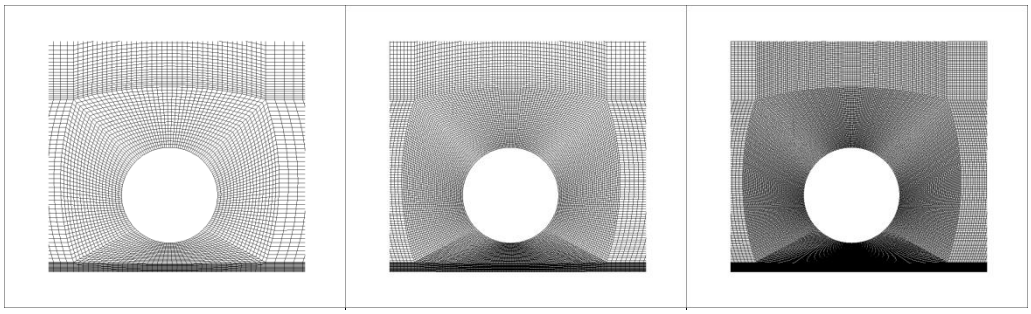

(a) (b) (c)

Fig. 2: (a) Coarse, (b) fine, and (c) very fine mesh schemes.

2.2 Governing Equations

Due to the low Mach number flow (Ma < 0.3) considered in this study, the flow is regarded as the incompressible two-dimensional flows assuming a constant fluid density. Thus, the continuity and momentum equations of the Navier-Stokes equations can be solved independent of the energy equation:

$$\frac{\partial \rho}{\partial t}+\frac{\partial \rho u_i}{\partial x_i}=0 \tag{1}$$

$$\frac{\partial \rho u_i}{\partial t}+\frac{\partial \rho u_i u_j}{\partial x_j}=-\frac{\partial p}{\partial x_j}+\mu\frac{\partial^2 u_i}{\partial x_j \partial x_j}, \tag{2}$$

Although the N–S equations can theoretically describe turbulence phenomena, the direct numerical simulation of turbulent flow using N–S equations is unrealistic especially in the high Reynolds number regime to resolve the Kolmogorov microscales related to the smallest eddies with the Reynolds number Re_η~1 based on their characteristic velocity υ and characteristic length η. Typically, the smallest scale of motion in a turbulent flow is in the order of 0.1 to 0.01 mm and frequencies around 10 kHz. Resolving eddies in large engineering flow problems with today's computers is a formidable task. Therefore, in practice, turbulence models are often employed to describe turbulence phenomena.

In this study, the laminar flow computation, the RANS and the LES approaches with their respective turbulence modes are utilized. The laminar flow computation is realized by discretizing the N–S equations with second-order difference schemes without a turbulence model. It is known that the dependence on turbulence modelling is reduced as the grid size decreases, since more turbulence is directly resolved. In the limit of infinitely fine grid density, the eddy viscosity approaches zero, which means all scales of eddies are directly resolved (Lee *et al.*, 2014). Therefore numerical solution of the N–S equations with sufficiently high precision can approximate turbulent flows to some extent. This is usually called the laminar approach (LAM) in commercial CFD packages. Singh and Mittal (2005) used this approach to study the drag crisis of the flow past a single cylinder. They found the results are comparable with the LES results. The RANS and LES approaches are introduced briefly as follows.

The RANS approach is probably the most popular method to simulate turbulent flow, because for most engineering purposes it is unnecessary to resolve the details of the turbulent fluctuations. The RANS equations are obtained by replacing the flow variables φ by the sum of a mean Φ and fluctuating components φ' ($\varphi=\Phi+\varphi'$) in the N–S equations and time-averaging to produce the resultant equations:

$$\frac{\partial \rho}{\partial t}+\frac{\partial \rho U_i}{\partial x_i}=0 \text{ and} \tag{3}$$

$$\frac{\partial \rho U_i}{\partial t}+\frac{\partial \rho U_i U_j}{\partial x_j}=-\frac{\partial p}{\partial x_j}+\mu\frac{\partial^2 U_i}{\partial x_j \partial x_j}+\frac{\partial(-\rho\overline{u_i' u_j'})}{\partial x_j}. \tag{4}$$

Turbulence modes are used to describe the Reynolds stresses, $-\rho\overline{u_i' u_j'}$, which can be expressed as follows based on the Boussinesq presumption that there exists an analogy between the action of viscous stresses and Reynolds stresses on the mean flow:

$$-\rho\overline{u_i' u_j'}=\mu_t\left(\frac{\partial U_i}{\partial x_j}+\frac{\partial U_j}{\partial x_i}\right)-\frac{2}{3}\rho k\delta_{ij} \tag{5}$$

The *k*–*ε* model is the most widely used and validated to represent $\mu_t=\rho C_\mu k^2/\varepsilon$. The *k*–*ω* model is used to give a more accurate prediction of the shedding of vortices than the *k*–*ε* model (Liang and Cheng, 2005). The *k*–*ω* model takes the turbulent frequency $\omega = \varepsilon/k$ as the second variable instead of the rate of dissipation of turbulence kinetic energy *ε*, and $\mu_t=\rho C_\mu k/\omega$. It is believed to have a better performance in the near-wall region because it does not require wall-damping functions in low Reynolds number applications. Menter (Versteeg and Malalasekera, 2007) suggested a hybrid SST model, using a transformation of the *k*–*ε* model to the *k*–*ω* model in the near-wall region and the standard *k*–*ε* model in the fully turbulent region far from the wall. This model offers improved performance with respect to adverse pressure gradients.

In RANS the collective behavior of all eddies must be described by a single turbulence model, but the problem dependence of the largest eddies complicates the search for widely applicable models. A different approach to the computation of turbulent flows accepts that the larger eddies need to be computed for each problem with a time-dependent simulation. The universal behavior of the smaller eddies, on the other hand, should be easier to capture with a compact model. This is the essence of the large eddy simulation (LES) approach to the numerical treatment of turbulence.

Instead of time-averaging the N–S equations, the LES uses spatial filtering to obtain the LES continuity and momentum equations:

$$\frac{\partial \rho}{\partial t}+\frac{\partial \rho\overline{u}_i}{\partial x_i}=0 \text{ and} \tag{6}$$

$$\frac{\partial \rho\overline{u}_i}{\partial t}+\frac{\partial \rho\overline{u}_i\overline{u}_j}{\partial x_j}=-\frac{\partial \overline{p}}{\partial x_j}+\mu\frac{\partial^2\overline{u}_i}{\partial x_j\partial x_j}-\left(\frac{\partial \rho\overline{u_i u_j}}{\partial x_j}-\frac{\partial \rho\overline{u}_i\overline{u}_j}{\partial x_j}\right). \tag{7}$$

The over bar indicates spatial filtering. Similar to the RANS approach, the SGS stresses:

$$\tau_{ij}\equiv\rho\overline{u_i u_j}-\rho\overline{u}_i\overline{u}_j=\underbrace{\left(\rho\overline{\overline{u}_i\overline{u}_j}-\rho\overline{u}_i\overline{u}_j\right)}_{1}+\underbrace{\rho\overline{\overline{u}_i u_j'}+\rho\overline{u_i'\overline{u}_j}}_{2}+\underbrace{\rho\overline{u_i' u_j'}}_{3}, \tag{8}$$

including on the right hand side the 1st (called Leonard stresses), 2nd (called cross-stresses), and 3rd (called LES Reynolds stresses) terms, need to be modeled in order to make the equations closed. For this purpose, the Smagorinksy–Lilly SGS turbulence model is employed:

$$\tau_{ij}=-2\mu_{SGS}\overline{S}_{ij}+\frac{1}{3}\tau_{ii}\sigma_{ij}=-\mu_{SGS}\left(\frac{\partial\overline{u}_i}{\partial x_j}+\frac{\partial\overline{u}_j}{\partial x_i}\right)+\frac{1}{3}\tau_{ii}\sigma_{ij}. \tag{9}$$

The SGS viscosity μ_{SGS} is evaluated as follows:

$$\mu_{SGS}=\rho(C_{SGS}\Delta)^2\sqrt{2\overline{S}_{ij}\overline{S}_{ij}}, \tag{10}$$

where Δ is the filter cutoff width, and the constant C_{SGS} is set to 0.1 in the present simulation, as is suggested by Versteeg and Malalasekera (2007).

2.3 Boundary conditions and numerical methods

A boundary condition of uniform velocity is applied at the inlet. For the laminar flow computation (LAM), no extra turbulence information is required. For the RANS and LES approaches, such information is essential. Similar to what was done by Doolan (2010), 1% turbulence intensity and a 5% turbulent viscosity ratio (μ_t/μ) at the inlet were employed in the RANS approach, while no velocity perturbations were introduced at the inlet in the LES approach. Doolan (2010) indicated that the free stream turbulence intensity has no influence on the frequency of the instabilities in the shear layer, although it does influence shear layer transition. In the case of the low and medium free stream turbulence intensities, the flow around and behind the cylinder is dominated by the intrinsic flow pattern around the cylinder rather than by the inflow turbulence. A symmetric boundary condition is applied to the top boundary by setting the vertical velocity to zero and applying a zero normal gradient condition for all other quantities (Brørs, 1999, Kazeminezhad *et al.*, 2010). The symmetric boundary condition is also applied at the short boundary in front of the leading point of the plane surface. Zero normal gradients for all parameters except pressure are applied at the outlet boundary. A no-slip velocity boundary condition is applied on the cylinder wall.

The finite volume method is employed to discretize the governing equations. For the incompressible flow, the continuity equation is simplified into a form in which the divergence of the velocity vanishes. Unlike the momentum equations, there is no transport or other equation for the pressure, though evidently the pressure field should be coupled with the velocity field. In the present study, a revised algorithm called SIMPLEC (Versteeg and Malalasekera, 2007) is used to solve the pressure–velocity coupling problem. For the spatial discretization of the governing equations in the convection–diffusion form, the diffusive fluxes are discretized using central differencing. For the convective fluxes, a second-order upwind scheme was employed in the LAM and SST models, and a bounded central differencing scheme was used in the LES model, as was suggested by Kim (2006).

An implicit second-order backward-differencing scheme for time-discretization was employed to advance the solution in time. The initial flow field used to start the simulation was a uniform velocity distribution with the incoming velocity of the inlet velocity and with a gauge pressure of 0 Pa. Using the well-recognized Strouhal number $St = fD/u_0 \approx 0.2$, one can estimate the vortex shedding frequency as $f \approx 10$ Hz, i.e., the period $T \approx 0.1$ s. A time step of $\Delta t = 0.05$ ms is chosen, with the dimensionless time step $\Delta t^* = u_0 \Delta t/D = 0.0025$, which is 1/2000th of the vortex shedding period. Lee *et al.* (2014) suggested at least 50 time steps per period are recommended to resolve the shedding physics correctly. Kazeminezhad *et al.* (2010) found that a dimensionless time step of ~0.02, i.e. around 250 time steps per period, is sufficient to obtain a reliable transient flow field.

The system of discretized governing equations is solved using a point-implicit, Gauss–Seidel relaxation along with an algebraic method to accelerate solution convergence. The solution was run for a non-dimensional time of $u_0 t/D = 250$, which is larger than the value of 76 used by Doolan (2010) and 100 suggested by Kim (2006), to establish a statistically steady state flow in the near-wake region. After that, the flow data of 5 s were recorded, which are enough to offer sufficient statistical information about the fluctuating forces. The frequency resolution is 0.2 Hz with a sampling duration of 5 s.

3. Numerical Results

3.1 Forces on the cylinder

First, the drag and lift forces on the cylinder, including the mean and fluctuation characteristics are examined to establish an understanding of the reliability and accuracy of flow simulation approaches. The drag and lift coefficients are defined by scaling the cylinder drag force F_D and lift force F_L with the free-stream velocity u_0 as follows:

$$C_D = \frac{F_D}{\rho u_0^2 D/2}, \; C_L = \frac{F_L}{\rho u_0^2 D/2}. \tag{11}$$

The mean drag and lift coefficients and their respective standard deviations are shown in Fig. 3. The mean values are represented by the bars. The standard deviation, in some literatures called root mean square (rms), was used to indicate the fluctuation while counteracting the mean value, as indicated by the symbols 'I' in Fig. 3. Three bars in each turbulence approach represent the results based on three mesh schemes, *i.e.*, the coarse, fine, and very fine mesh as mentioned in the previous section. Overall, the numerical results of different

turbulence models and different meshes are in the same order of magnitude, except for some cases of the SST model, which will be explained further at a later stage when the detailed flow fields are examined.

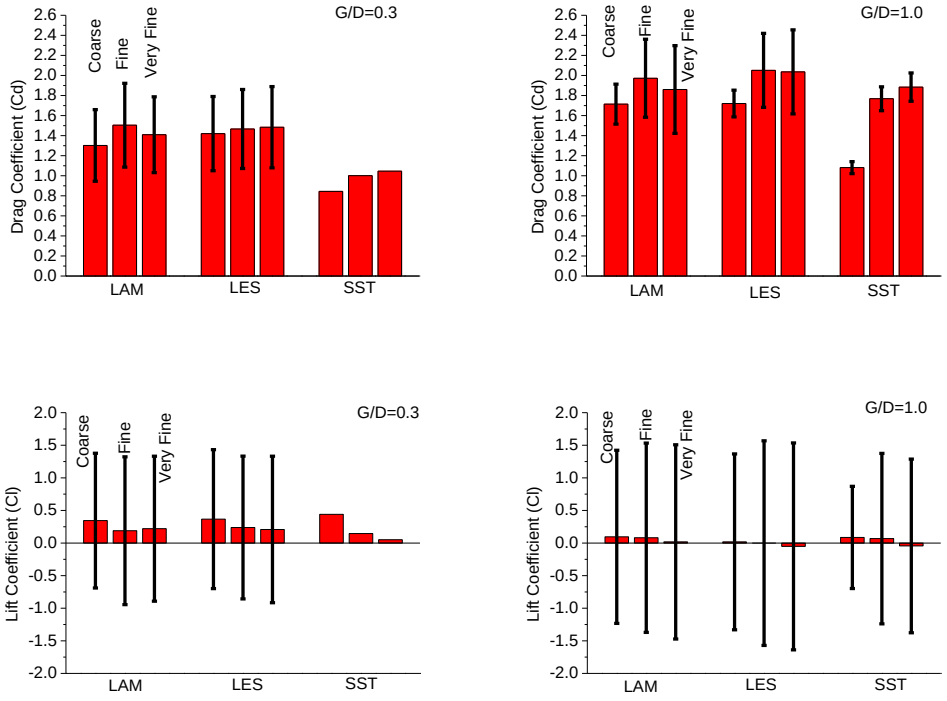

Fig. 3: The mean values and standard deviations of the drag and lift coefficients.

The mean drag force coefficients of the cylinder predicted with the coarse-mesh scheme are different from those from the finer-mesh schemes. This is because the coarse mesh cannot resolve the flow details. One can also notice that the drag forces obtained by the LAM and LES approaches are quite close to each other and that they have appreciable differences from the results of the SST model. For the case of G/D = 0.3, the mean drag coefficient obtained by the LAM and LES approaches is around 1.3–1.5, and it rises to 1.7–2.0 at G/D = 1.0. The results of the SST model show that the drag coefficient is approximately 1.0 at G/D = 0.3, and 1.8 at G/D = 1.0. This tendency agrees with most previous experimental and numerical results, such as those of Lei *et al.*(1999) and Kazeminezhad *et al.* (2010). Experimental results for C_D are 1.1–1.5 in the case of a single cylinder at the subcritical regime with the Reynolds numbers in the range of 1.0×10^4 –1.0×10^5 (Sumer and Fredsoe, 2006) The numerical C_D obtained in the present study is a little larger than the experimental data as was in the 2-D calculation results of Tutar and Holdø (2001), where C_D = 1.4–1.47 was predicted. This may be due the fact that in a 2-D simulation the spanwise effect is ignored. The 2-D simulation assumes that the flow is uniform in the axial direction of the cylinder, which will cause an increase in the drag force.

The standard deviation of the drag coefficients shows that the drag fluctuations predicted by the LAM and LES approaches are about 10–30% of the mean drag forces. The drag fluctuations predicted by the coarse mesh model are lower than those by models with fine and very fine meshes, indicating that the coarse mesh cannot adequately resolve the transient flow pattern. It is interesting to find that the standard deviations vanish for G/D = 0.3, showing no fluctuations at all. It will be seen in the following subsection that no vortex shedding was predicted by the SST approach at G/D = 0.3.

Unlike the mean drag coefficient, which is rather stable in all predictions, the mean lift coefficient varies significantly with the different mesh schemes and turbulence models. The drag is ascribed to the appreciable pressure difference between the front region of the cylinder, where flow stagnation occurs, and the wake region, while lift is ascribed to the pressure difference between the up and down surfaces of the cylinder. Due to vortex shedding, the pressure distribution pattern on the up and down surfaces of the cylinder alternates, resulting in the lift force fluctuations. For an isolated cylinder, the mean lift is theoretically zero. However, for a cylinder above a plane surface, the mean lift force does not vanish for small G/D and is positive (directed away from the plane

surface), as observed in the previous experiment (Sumer and Fredsoe, 2006). The lift coefficients are shown in Fig. 3. As can be seen, the lift coefficient reduces dramatically from G/D = 0.3 to G/D = 1.0. This phenomena was also found in the numerical results of Kazeminezhad *et al.* (2010). The measured mean lift coefficients of G/D = 0.3 and G/D = 1.0 by Buresti and Lanciotti (1992) are approximately 0.2 and 0.03, respectively, in the subcritical regime. Among all the simulated results, the LES and LAM show better agreement with the experimental data.

The large standard deviation in the predicted lift coefficient in Fig. 3 is due to the fact that the mean lift force is very small while its fluctuations are very large. Thus, a precise estimation of the mean lift coefficient is difficult. This observation is also supported by previous experimental results. For example, the mean lift force was found to be all positive in the results of Buresti and Lanciotti (1992), while some negative lift forces were also detected in some cases (Lei *et al.*, 1999).

The lift fluctuation predicted by the 2-D simulations is around 1.0~1.1 for G/D = 0.3, and 1.4~1.6 for G/D = 1.0, which are much larger than the experimental results, which are between 0.1~0.2 and 0.2~0.3 respectively (Sumer and Fredsoe, 2006). This may be ascribed to the intrinsic deficiency of a 2-D simulation, where the flow correlation in the spanwise direction is not taken into account. A 2-D simulation assumes that vortexes along the cylinder are shedding simultaneously, resulting in the increase of the lift fluctuations. A large lift fluctuation was also obtained in Lee *et al.* (2014) where a small span length 2D was adopted. They found that change in the cylinder span length does not affect drag and Strouhal number considerably, whereas it affects lift quite significantly. The spanwise correlations drop significantly as the span length increases, so is the lift coefficient. They argued that a span length of 16D is needed to predict physically correct spanwise correlations. There are no lift fluctuations in the SST results in the case of G/D = 0.3 owing to the fact that no vortex shedding is predicted. At G/D = 1.0, the fluctuation levels obtained by SST are in the same order as those obtained by the LAM and LES approaches.

The spectra of the drag and lift fluctuations are shown in Fig. 4 to Fig. 7. The results of the SST approach in the case of G/D = 0.3 are omitted because no vortex shedding is predicted, leading to no fluctuations of the drag and lift forces on the cylinder. The frequency is non-dimensionalized by multiplying D/u_0. The fluctuations are mainly located in the non-dimensional frequency range of 0.2–0.3, where the Strouhal number is supposed to fall into. At G/D = 0.3, the fluctuation at one-half of the Strouhal number is also obvious. For the drag force, fluctuations at the Strouhal number and its second harmonic are predominant. The 2nd harmonic of the vortex shedding frequency is due to the fact that the vortexes are shedding on both the up and down sides of the cylinders, leading to drag fluctuations at twice the vortex shedding frequency. Especially in the case of G/D = 1.0 in the SST model, the drag spectra are very clean, with components at the vortex shedding frequency and its low harmonics. This indicates that the RANS approach predicts a well-organized and periodic flow pattern at this Reynolds number. This is due to the intrinsic property of RANS approach: when the turbulence model is used, the diffusion term is increased by the added turbulent viscosity and the numerical stability is guaranteed, however high frequency fluctuations as well as small eddies (high wave-number fluctuations) will be smoothed out.

It can be seen that the coarse mesh scheme also produces a very regular vortex shedding frequency in the LAM and LES models at G/D = 1.0. This demonstrates that the mesh resolution is not fine enough to capture the turbulent flow and therefore only potential flow results are arrived at. There were no fluctuations in the drag and lift spectra in the SST model at G/D = 0.3, indicating no vortex shedding was predicted. This will be further explained in the next subsection, where the flow patterns will be shown. From the drag and lift fluctuation spectra, it can also be seen that the results of the LAM and LES approaches are quite similar, indicating that, with a sufficiently high mesh resolution, a numerical solution of the N–S equations without turbulence models can yield the unsteady flow reasonably as was found by Singh and Mittal (2005).

The estimation of the Strouhal number and judgment of the onset and suppression of vortex shedding can be determined by different methods. In this study, the estimation is based on an observation of the spectrum of the lift coefficient (Lei *et al.*, 1999), since each vortex shedding is accompanied by a lift fluctuation. Many studies have shown that the vortex shedding frequency is insensitive to G/D, once vortex shedding occurs (Choi and Lee, 2000, Lei *et al.*, 1999, Oner *et al.*, 2008); the Strouhal number remains constant at ~0.2 and is identical with that in a uniform flow without the plane wall. From the lift spectra, it can be seen that the peaks fall in a normalized frequency range of 0.2–0.3, and, with an increase of the mesh resolution, more spikes appear around this range, indicating that smaller size vortices are captured. For G/D = 1.0, the predicted Strouhal number decreases and is closer to 0.2 as the mesh resolution increases. This is especially obvious when going from the coarse mesh scheme to the fine mesh scheme, but from the fine scheme to the extremely fine scheme little

change in the Strouhal number was found, showing the second mesh scheme is sufficiently fine to resolve the flow structures.

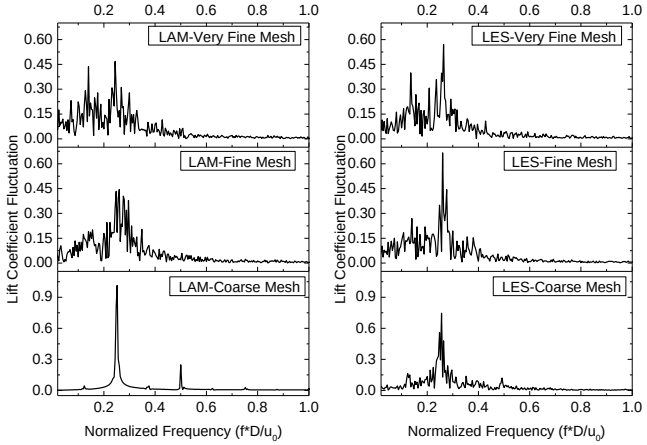

Fig. 4: Fluctuations of the lift coefficient at $G/D = 0.3$.

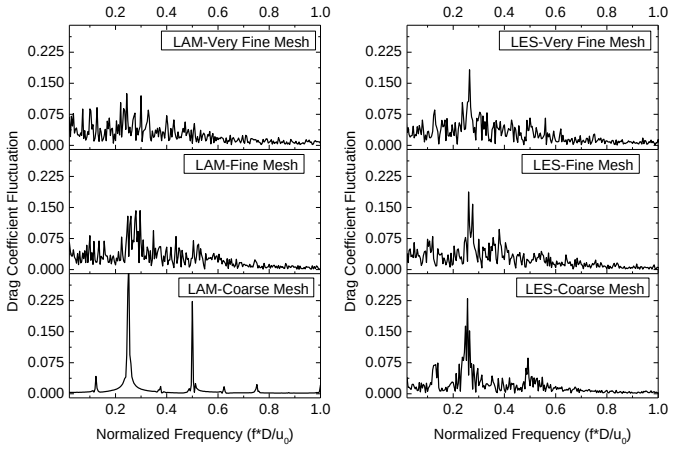

Fig. 5: Fluctuations of the drag coefficient at $G/D = 0.3$.

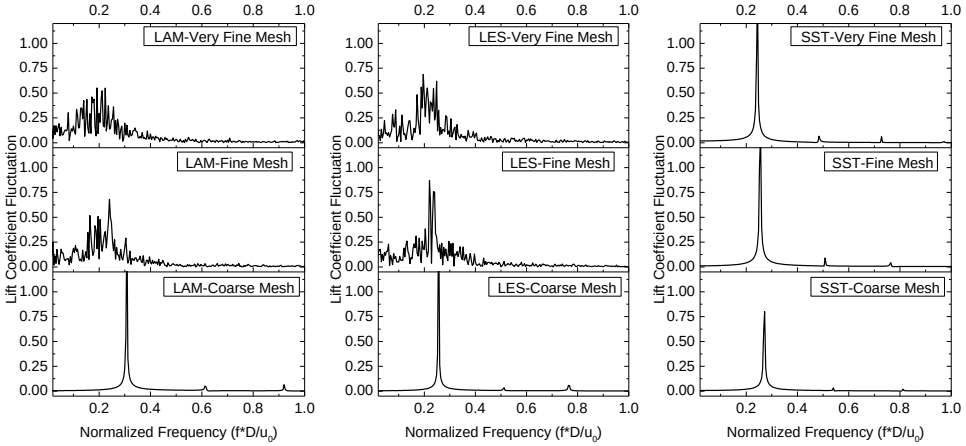

Fig. 6: Fluctuations of the lift coefficient at $G/D = 1.0$.

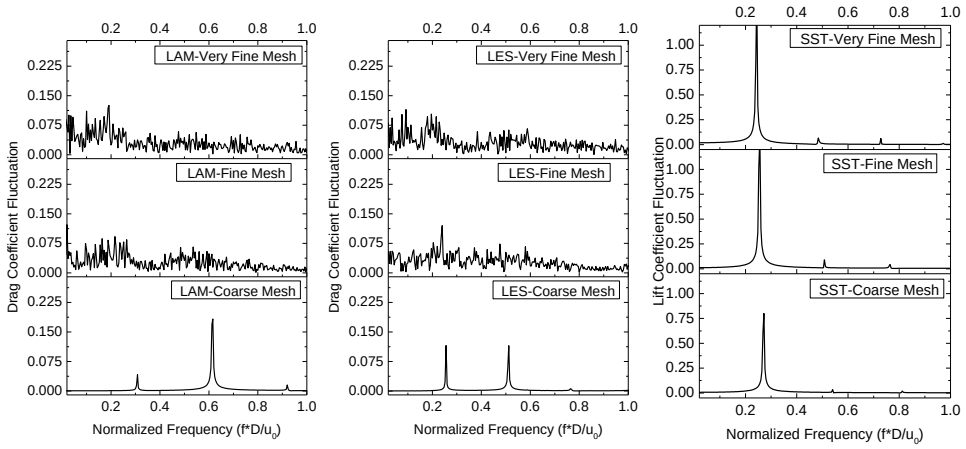

Fig. 7: Fluctuations of the drag coefficient at $G/D = 1.0$.

3.2 Flow structures

The previous subsection shows that the numerical results are more sensitive to the turbulence models than the mesh resolution, as long as the mesh is sufficiently fine. Therefore only the flow fields of the fine mesh scheme are discussed in this section. The mean pressure distribution and the stream traces based on the mean velocities are shown in Fig. 8. The pressure in front of the cylinder is higher than in the wake region behind the cylinder as a result of stagnation of the flow. On the upper and down sides of the cylinder, low pressure regions exist due to the flow acceleration. The pressure distribution around the cylinder is not symmetric due to the plane wall influence in the case of $G/D = 0.3$ with the stagnation point on the lower front part, while for $G/D = 1.0$ it is almost symmetric with the stagnation point very close to the cylinder front tip.

For $G/D = 0.3$, The flow structures behind the cylinder found with the LAM and LES approaches are more complicated than those from the SST approach. In fact, the LAM and LES results show that, besides the major eddy pair behind the cylinder, there are some secondary eddies, as via experiments (Oner *et al.*, 2008), while in the SST results based on the RANS equations, no secondary eddies exist. The upwash created by the wall behind the cylinder is obvious: the wake regions in the LAM and LES results are mainly on the upper part of the cylinder indicating that the plane wall forces the wake flow upward; In absence of the plane wall, *i.e.*, just a single cylinder, the time-averaged wake flow is symmetric about the cylinder. When the flow past the cylinder, it expands, but due to the restriction of the plane wall the lower part can be substantially affected. Vortices exist under the wake region near the plane wall in the LAM and LES approaches, acting as obstacles push the wake up. Vortices are absent in the SST turbulence approach, but the upwash of the wake by the plane wall is still noticeable through the slightly skewed asymmetric streamlines in the wake. For $G/D = 1.0$ the average streamlines of the three approaches are more similar compared with the case of $G/D = 0.3$, and the flow structure are close to symmetric meaning that the influence of the plane wall in this case is very weak.

Snapshots of the vorticity distribution are shown in Fig. 9. The boundary layer formed along the cylinder contains a significant amount of vorticity, as can be easily seen in the vorticity contours. Intense vorticity exists on the up and down sides of the cylinder. The vorticity on the up side is in the clockwise direction, while on the down side it is in the counter-clockwise direction. When the Reynolds number is high enough, the boundary layer over the cylinder surface will separate owing to the adverse pressure gradient imposed by the divergent geometry of the flow environment at the rear side of the cylinder. Due to the separation of boundary layers, a shear layer is formed, as can be seen clearly in vorticity contours. The vorticity is fed into the shear layer formed downstream of the separation point and may cause the shear layer to roll up into a vortex with a sign identical to that of the incoming vorticity. The pair of up and down shear layers is unstable, and vortex shedding can occur when the two shear layers interact with each other. When the larger vortex at one side becomes strong enough to draw the opposing vortex across the wake, the supply of vorticity to the larger vortex from its boundary layer will be cut off by the approach of the opposing vortex, resulting in the shedding of the larger vortex. This phenomenon occurs in almost all cases shown, as can be seen in the velocity vectors and vorticity contours, where the two shear layers bend toward each other. The exception is the SST model at $G/D = 0.3$, in which the shear layers are almost straight.

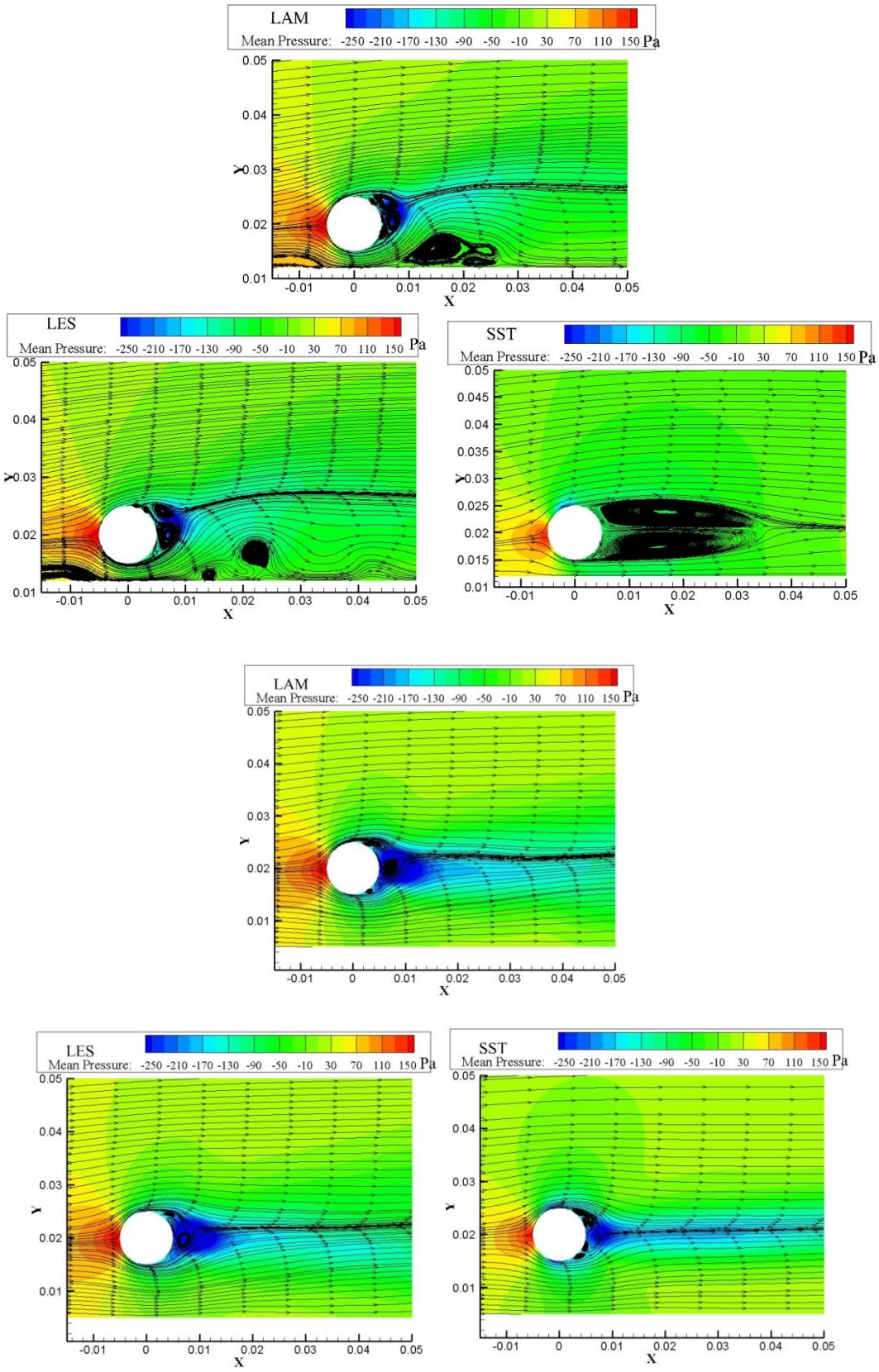

Fig. 8: The mean pressure distribution and stream traces.

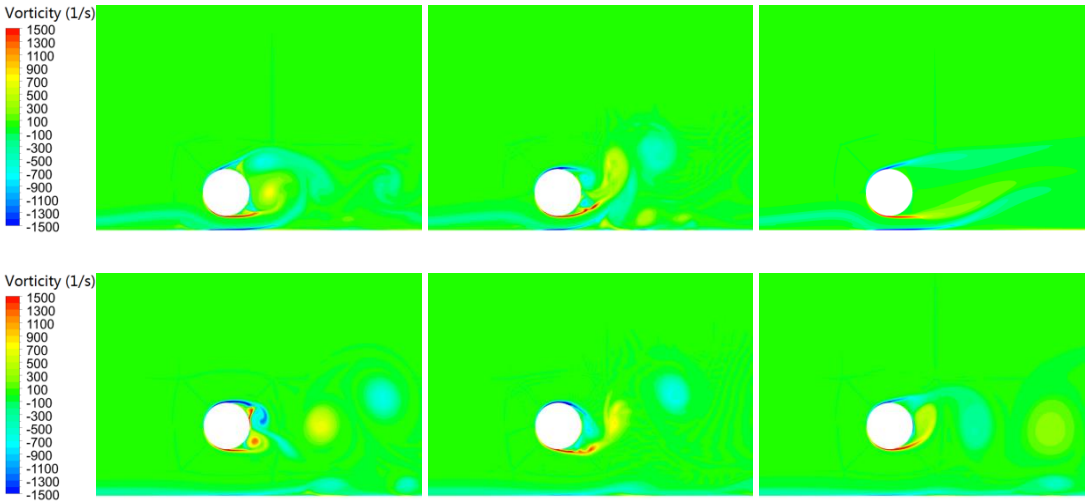

Fig. 9: An instantaneous distribution of the vorticity: left: LAM; middle: LES; and right: SST.

3.3 Wall pressure and shear stress on the plane surface

Since the results predicted by the LES have a better agreement with the experimental results for unsteady flow fields around the cylinder, the LES is used to study the pressure and shear stress on the plane surface. The mean distributions of the pressure and the shear stress in the *x* direction on the plane surface in the duration of 1 minute are shown in Fig. 10. The pressure and shear stress were non-dimensionalized by $\rho u_0^2 / 2$. In front of the cylinder, the pressure on the wall boundary increases as the flow approaches the cylinder, while the amplitude of the shear stress decreases slightly. In the downstream region, both the pressure and the shear stress wiggle violently along the wall boundary, especially for the case of G/D = 0.3. Previous study using the RANS approach with the *k-ε* turbulence model (Ong *et al.*, 2010) showed that the mean pressure distribution was quite smooth. The above discussions indicate that the flow structure is complex, and this will lead to the fluctuation of the forces on the cylinder and plane surfaces as well.

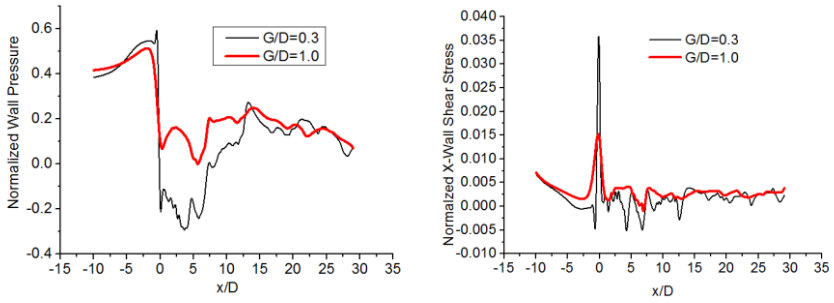

Fig. 10. Distributions of (left) mean pressure and (right) shear stress on the plane surface.

Six points with x-coordinates of −3.0*D*, −1.0*D*, 0.0*D*, 1.0*D*, 3.0*D*, and 6.0*D* from the center of the cylinder (*x* = 0) were selected on the plane surface for examining the spatial and frequency properties of the surface forces. The frequency spectra of the pressure and shear stress were obtained via Fourier transforms of the recorded data, and are shown in Figs. 10 and 11. The DC components were omitted in the figures, because only the fluctuating components are important in flow-induced boundary vibration and sound radiation.

The pressure and shear stress components are found to have large amplitudes in the low frequency range. When the non-dimensional frequency is greater than 0.4, which is approximately twice the Strouhal number, the amplitude becomes negligibly small. The amplitude of the pressure is approximately two orders of magnitude larger than that of the shear stress. It is known from boundary layer theory that the static pressure is constant across the thin boundary layer and is equal to the static pressure at the outer edge of the boundary layer, which can be approximately predicted by an inviscid flow solution. Therefore, the pressure fluctuation on the plane boundary is directly related to the main flow where vortex motion exists. However, the shear stress fluctuation is

determined by $\mu\partial u_x/\partial y=0$ on the wall and, due to the viscosity in the boundary layer, it can be substantially smaller than that outside the boundary layer, where its fluctuation is expected to be of the same order as the pressure fluctuations.

In the spectra of pressure fluctuation, one can see that at the locations of x = 0.0D and 1.0D, the components have peak values at the vortex-shedding frequency. For the positions beyond 3.0D, the components at the vortex-shedding frequency gradually decrease. At 6.0D, the fluctuations at frequencies lower than the vortex-shedding frequency even overweigh the component near the Strouhal number. Upstream of the cylinder (at x = −1.0D), the component is also discernible at the vortex-shedding frequency, although its amplitude is much smaller compared with those at x = 0.0D and 1.0D. At the location of x = −3.0D upstream, the fluctuations become very weak. This phenomenon indicates that the effects of vortex shedding on the force fluctuations on the plane wall surface are mainly confined to 3.0D downstream and 1.0D upstream, and beyond this region the effects become very small.

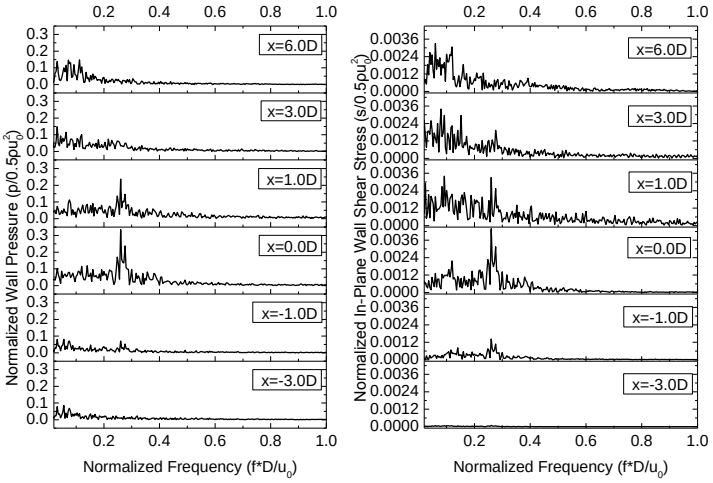

Fig. 11: Spectra of pressure (left) and shear stress (right) fluctuations on the plane wall at G/D = 0.3.

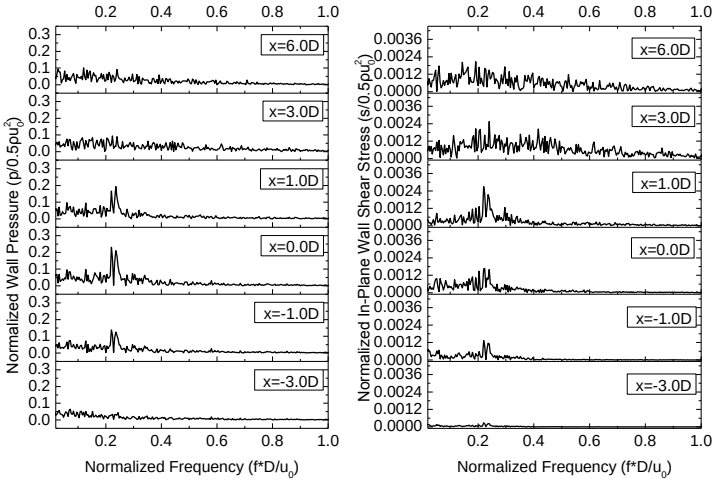

Fig. 12: Spectra of pressure (left) and shear stress (right) fluctuations on the plane wall at G/D = 1.0.

It is worth pointing out that, to zero pressure gradient turbulent boundary layer flows, it is generally accepted that the fluctuation magnitude of wall-shear stress $\tau_{w,rms}$ is around 0.4 of the mean shear stress $\overline{\tau}_w$ (Colella and Keith, 2003, Örlü and Schlatter, 2011). For G/D = 1.0, $\tau_{w,rms}/\overline{\tau}_w$ at −3.0D, −1.0D, 0.0D, 1.0D, 3.0D, and 6.0D are 0.33, 0.34, 0.15, 11.0, 3.02, 2.41, respectively. The upstream values are close to 0.4 indicating that the effect of the cylinder on the upstream wall stress is small. The large values of $\tau_{w,rms}/\overline{\tau}_w$ at the downstream demonstrating the cylinder have certain influence on the downstream wall shear stress.

To investigate the spatial correlations of the surface pressure and shear stress, the coherence functions of the pressure and shear stress at each monitoring position with respect to those at $x = 0D$ are presented in Fig. 13 for $G/D = 1.0$. The spatial coherence value of pressure is higher than that of the shear stress, indicating that the pressure fluctuation is more correlated than the shear stress fluctuation. This is clearly shown by the mean coherence value in the normalized frequency band of 0 – 2. If a threshold value of 0.55 is set, then only the pressure fluctuations at the locations of $x = \pm 1.0D$ are correlated to $x = 0.0D$, and the shear stress fluctuations are not well correlated.

For the pressure fluctuation, due to the fact that the pressure in the boundary layer is (almost) equal to that outside the boundary layer at the same x-coordinate ($\partial p/\partial y=0$), the correlation of the pressure fluctuations is retained. The coherence values of the pressure fluctuations at monitoring points $x = -1.0D$ and $1.0D$ with the reference point $x = 0.0D$ are close to 1.0, which shows that they are well correlated. The pressure fluctuations at $x = -3.0D$ and $3.0D$ with the reference point $x = 0.0D$ are weakly correlated, as shown by their low coherence value, especially in the higher frequency range (normalized frequency > 1.0). This is reasonable because, as discussed above, the range of influence of vortex shedding is mainly restricted to $x = -1.0D$ to $3.0D$, and beyond this range the random nature of turbulent flow plays an important role. Thus, the force fluctuations in this range are expected to be uncorrelated with the one at the reference point of $x = 0.0D$. For the shear stress, the complex flow structures affect the wall shear stress through the boundary layer. Although the flow structure outside the boundary layer is quite complex owing to the vortex shedding and the flow structure is correlated in the vortex region, due to the viscosity effect of the boundary layer this correlation between the transmitted flows into the boundary layer is dramatically reduced.

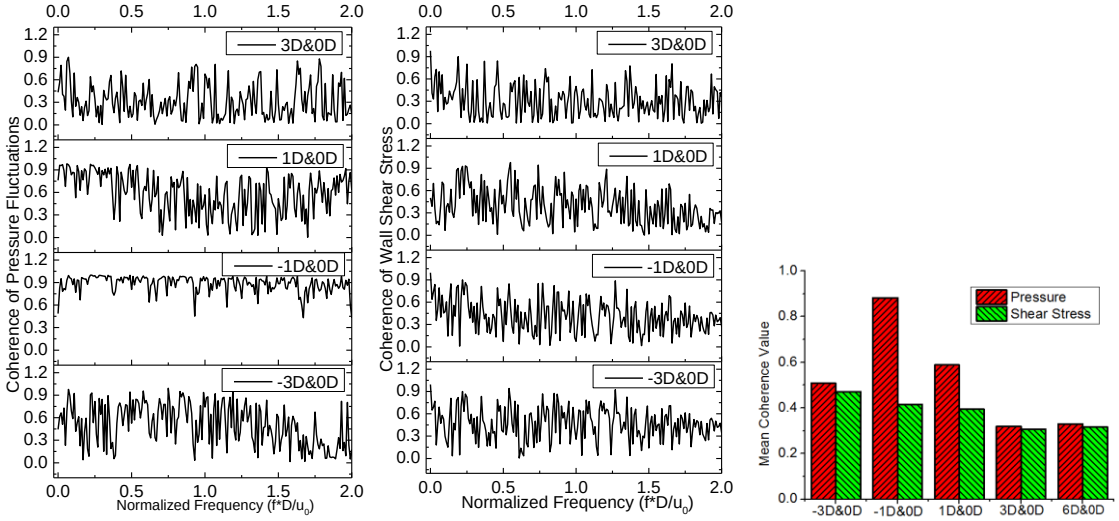

Fig. 13: Coherence functions of the pressure and shear stress fluctuations on the plane wall at $G/D = 1.0$.

4. Conclusion

In this paper, the fluctuating pressure and shear stress on a plane surface located beneath a circular cylinder have been numerically studied in the subcritical flow regime in 2-D sense using different turbulence approaches, namely the computation without any turbulence model (or the laminar approach, LAM), the large eddy simulation (LES), and the Reynolds-averaged Navier-Stokes equations (RANS) approach with shear-stress transport (SST) model. The overall results are reasonable; the mean drag and lift coefficients of the cylinder, and the Strouhal number were found to be consistent with previous experimental results. The 2-D large eddy simulation (LES), though there exist controversial opinions with its application, displayed good performance in this study for the investigated subcritical regime of flow around cylinder with Re = 5000. The main observations are summarized as follows:

- The LES approach produced the most accurate lift force on the cylinder and a detailed flow pattern in the wake region. The flow structure obtained via the RANS approach was quite regular. At $G/D = 1.0$, vortices were shed systematically, leading to regular drag and lift fluctuations with distinct spikes at the Strouhal number and its harmonics. However, at $G/D = 0.3$, no vortex shedding was predicted even though it

occurred in the laminar (LAM) and LES models. For G/D = 0.3 the asymmetric mean flow fields clearly show the upwash created by the plane wall, while for G/D = 1.0 the almost symmetric mean flow fields indicate that the effect of the wall is very weak.

- The mesh resolution had a noticeable effect on the flow structure. When the mesh resolution was not fine enough, no turbulent flow could be observed. With a more refined mesh, the Strouhal number decreased and became closer to the experimental value of 0.2. When the mesh resolution was sufficiently high, the LAM approach (without any turbulence model) could predict the turbulent flow around the cylinder at a moderate Reynolds number reasonably.
- The force fluctuation on the plane surface was mostly significant below twice the vortex-shedding frequency, and the amplitude of the pressure fluctuations was approximately two orders of magnitude larger compared with the amplitude of the stress force fluctuations. The fluctuations were mainly confined to a distance of three cylinder diameters downstream and one diameter upstream of the cylinder, indicating that the effects of vortex shedding behind the cylinder on the plane wall force were confined to this region. The surface pressure fluctuations in the range of one diameter upstream and downstream of the center of the cylinder were spatially well correlated, and became less coherent as the distance to the cylinder center increased. The in-plane shear force fluctuations were spatially less correlated compared with that of the pressure fluctuations.

This study also showed that in a 2-D simulation the force fluctuations on the cylinder were much higher than those from experimental measurements. This may be attributed to the fact that the spanwise flow correlation effect was ignored, i.e., it assumed that all the vortexes along the cylinder were shed simultaneously. Therefore, a more accurate and universal fully 3-D turbulent flow simulation, especially an LES, will be conducted to study the characteristics of 3-D statement of flow consideration in the near future.

Acknowledgement

This work was partially completed while the first author was on sabbatical leave at the Centre for Acoustics, Dynamics and Vibration of The University of Western Australian. The first author kindly acknowledges the support of the National Natural Science Foundation of China (Project Numbers: 51306163, 51575497). The authors are grateful for the financial support from the CRC for Infrastructure Engineering Asset Management (CIEAM).

References

Bouris, D. and Bergeles, G. (1999): 2D LES of vortex shedding from a square cylinder, Journal of Wind Engineering and Industrial Aerodynamics, 80(1–2), pp.31-46. http://doi.org/10.1016/S0167-6105(98)00200-1

Brørs, B. (1999): Numerical modeling of flow and scour at pipelines, Journal of Hydraulic Engineering, 125(5), pp.511-523. http://dx.doi.org/10.1061/(ASCE)0733-9429(1999)125:5(511)

Buresti, G. and Lanciotti, A. (1992): Mean and fluctuating forces on a circular cylinder in cross-flow near a plane surface, Journal of Wind Engineering and Industrial Aerodynamics, 41(1–3), pp. 639-650. doi:10.1016/0167-6105(92)90476-Q

Choi, J. H. and Lee, S. J. (2000): Ground effect of flow around an elliptic cylinder in a turbulent boundary layer, Journal of Fluids and Structures, 14(5), pp. 697-709. doi:10.1006/jfls.2000.0290

Colella, K. J. and Keith, W. L. (2003): Measurements and scaling of wall shear stress fluctuations, Experiments in Fluids, 34(2), pp.253-260. doi:10.1007/s00348-002-0552-2

Doolan, C. J. (2010): Large eddy simulation of the near wake of a circular cylinder at sub-critical Reynolds number, Engineering Applications of Computational Fluid Mechanics, 4(4), pp.496–510. doi:10.1080/19942060.2010.11015336

Kazeminezhad, M. H., Bakhtiary, A. Y. and Shahidi, A. E. (2010): Numerical investigation of boundary layer effects on vortex shedding frequency and forces acting upon marine pipeline, Applied Ocean Research, 32(4), pp.460-470. doi:10.1016/j.apor.2010.10.002

Kim, S. E. (2006): Large eddy simulation of turbulent flow past a circular cylinder in subcritical regime, 44th AIAA Aerospace Sciences Meeting and Exhibit, Reno,Nevada, USA. http://dx.doi.org/10.2514/6.2006-1418

Lee, A. H., Campbell, R. L. and Hambric, S. A. (2014): Coupled delayed-detached-eddy simulation and structural vibration of a self-oscillating cylinder due to vortex-shedding, Journal of Fluids and Structures, 48(7), pp.216–234. doi:10.1016/j.jfluidstructs.2014.02.019

Lei, C., Cheng, L. and Kavanagh, K. (1999): Re-examination of the effect of a plane boundary on force and vortex shedding of a circular cylinder, Journal of Wind Engineering and Industrial Aerodynamics, 80(3), pp.263-286. doi:10.1016/S0167-6105(98)00204-9

Liang, D. and Cheng, L. (2005): Numerical modeling of flow and scour below a pipeline in currents: Part I. Flow simulation, Coastal Engineering, 52(1), pp.25-42. doi:10.1016/j.coastaleng.2004.09.002

Liang, D., Cheng, L. and Li, F. (2005): Numerical modeling of flow and scour below a pipeline in currents: Part II. Scour simulation, Coastal Engineering, 52(1), pp.43-62. doi:10.1016/j.coastaleng.2004.09.001

Liu, B., Feng, L., Nilsson, A. and Aversano, M. (2012): Predicted and measured plate velocities induced by turbulent boundary layers, Journal of Sound and Vibration, 331(24), pp.5309-5325. http://dx.doi.org/10.1016/j.jsv.2012.07.012

Murakami, S. and Mochida, A. (1995): On turbulent vortex shedding flow past 2D square cylinder predicted by CFD, Journal of Wind Engineering and Industrial Aerodynamics, 54–55, pp.191-211. https://doi.org/10.1016/0167-6105(94)00043-D

Oner, A. A., Kirkgoz, M. S. and Akoz, M. S. (2008): Interaction of a current with a circular cylinder near a rigid bed, Ocean Engineering, 35(14–15), pp.1492-1504. http://doi.org/10.1016/j.oceaneng.2008.06.005

Ong, M. C., Utnes ,T., Holmedal, L. E., Myrhaug, D. and Pettersen, B. (2010): Numerical simulation of flow around a circular cylinder close to a flat seabed at high Reynolds numbers using a *k–ε* model, Coastal Engineering, 57(10), pp.931-947. doi:10.1016/j.coastaleng.2010.05.008

Örlü, R. and Schlatter, P. (2011): On the fluctuating wall-shear stress in zero pressure-gradient turbulent boundary layer flows, Physics of Fluids, 23(2), pp.557-583. http://dx.doi.org/10.1063/1.3555191

Price, S. J., Sumner, D., Smith, J. G., Leong, K. and PaÏDoussis, M. P. (2002): Flow visualization around a circular cylinder near to a plane wall, Journal of Fluids and Structures, 16(2), pp.175-191. doi:10.1006/jfls.2001.0413

Rahman, M. M., Karim, M. M., and Alim, M. A, (2007): Numerical investigation of unsteady flow past a circular cylinder using 2-D finite volume method, Journal of Naval Architecture and Marine Engineering 4(1): 27-42. http://dx.doi.org/10.3329/jname.v4i1.914

Rodi, W. (1993): On the simulation of turbulent flow past bluff bodies, Journal of Wind Engineering and Industrial Aerodynamics, 46–47, pp.3-19. doi:10.1016/0167-6105(93)90111-Z

Singh, S. P. and Mittal, S. (2005): Flow past a cylinder: shear layer instability and drag crisis, International journal for numerical methods in fluids, 47(1) pp.75-98. doi:10.1002/fld.807

Stringer, R. M., Zang, J. and Hillis, A. J. (2014): Unsteady RANS computations of flow around a circular cylinder for a wide range of Reynolds numbers, Ocean Engineering, 87(17-18), pp.1-9. doi:10.1016/j.oceaneng.2014.04.017

Sumer, B. M. and Fredsoe, J. (2006): Hydrodynamics around cylindrical structures. Singapore, World Scientific Publishing Co. Pte. Ltd.

Tutar, M. and Holdø A. (2001): Computational modelling of flow around a circular cylinder in sub-critical flow regime with various turbulence models, International Journal for Numerical Methods in Fluids, 35(7), pp.763-784. doi:10.1002/1097-0363(200`10415)35:7<763::AID-FLD112>3.0.CO;2-S

Versteeg, H. K. and Malalasekera, W. (2007): An introduction to computational fluid dynamics: The finite volute method, 2nd edition, Essex, UK, Pearson Education Limited.